ACS APPLIED MATERIALS & INTERFACES

Research Article

www.acsami.org

Silver Iodide Microstructures of a Uniform Towerlike Shape: Morphology Purification via a Chemical Dissolution, Simultaneously Boosted Catalytic Durability, and Enhanced Catalytic Performances

Bin Lei,[†,‡] Mingshan Zhu,[‡] Penglei Chen,*[,†,‡] Chuncheng Chen,[‡] Wanhong Ma,[‡] Tiesheng Li,*[,†] and Minghua Liu*[,‡]

[†]College of Chemistry and Molecular Engineering, Zhengzhou University, 100 Science Road, Henan, Zhengzhou 450001, People's Republic of China

[‡]Beijing National Laboratory for Molecular Science, CAS Key Laboratory of Colloid, Interface and Chemical Thermodynamics, Institute of Chemistry, Chinese Academy of Sciences, No. 2 Zhongguancun Beiyijie, Beijing 100190, People's Republic of China

Supporting Information

ABSTRACT: The fabrication of microstructures/nanostructures of a uniform yet well-defined morphology has attracted broad interest from a variety of fields of advanced functional materials, especially catalysts. Most of the conventional methods generally suffer from harsh synthesis conditions, requirement of bulky apparatus, or incapability of scalable production, etc. To meet these formidable challenges, it is strongly desired to develop a facile, cost-effective, scalable method to fulfill a morphology purification. By a precipitation reaction between $AgNO_3$ and KI, we report that irregular AgI structures, or their mixture with towerlike AgI architectures could be fabricated. Compared to the former, the mixed structures exhibit enhanced catalytic reactivity toward the photodegradation of Methyl Orange pollutant. However, its catalytic durability, which is one of the most crucial criteria that are required by superior catalysts, is poor. We further show that the irregular structures could be facilely removed from the mixture via a KI-assisted chemical dissolution, producing AgI of a uniform towerlike morphology. Excitingly, after such simple morphology purification, our towerlike AgI displays not only a boosted catalytic durability but also an enhanced catalytic reactivity. Our chemical dissolution-based morphology purification protocol might be extended to other systems, wherein high-quality advanced functional materials of desired properties might be developed.

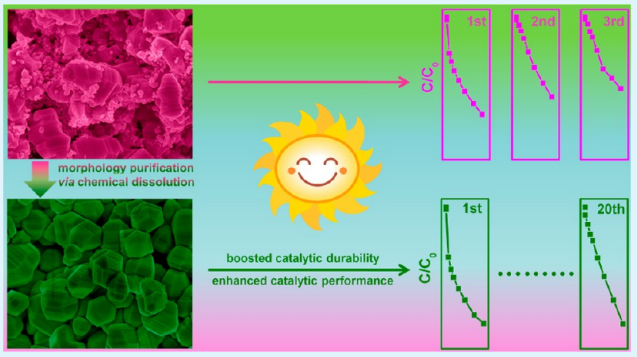

KEYWORDS: *morphology purification, boosted catalytic durability, enhance catalytic reactivity, chemical dissolution, visible-light/sunlight-driven photocatalysts*

1. INTRODUCTION

Recently, microstructures/nanostructures of a well-defined yet uniform morphology have attracted broad interest. This stems from their interesting shape-dependent properties, which provide them with abundant opportunities as advanced functional materials in a wide variety of fields, including sensor, energy harvesting/conversion/storage, optoelectronics, catalysts, etc.[1−12] First, advanced functional materials of a uniform morphology endow researchers with an ideal model scientific forum to disclose the correlation between morphology and function, which is an issue of general concern in modern materials science. Second, by taking the advantage of this issue, an optimized selection of innovative advanced functional materials with desired properties might be developed.[1−12]

To realize these issues, one of the most critical prerequisites is to obtain well-defined microstructures/nanoarchitectures of a uniform morphology. In this regard, two strategies are frequently employed.[13−30] The first way is a controllable synthesis, which could be realized by capping agent-assisted fabrication, seed/template-directed fabrication, etc., or by a strict adjustment of the synthesis parameters. Nevertheless, the use of diverse templates, seeds, capping agents, or the involvement of numerous chemical reagents, commonly makes this protocol a tedious work.[14] Meanwhile, it sometimes is necessary that the fabrication has to be performed with an accurate consideration of the experimental parameters, since only a slight change in the synthesis conditions would lead to products of distinct morphologies.[29,30] As a complementary protocol, a post-treatment of the structures is another way to achieve a uniform morphology.[13] Several sophisticated methods, including diverse variants of chromatography, centrifugation, electrophoresis, filtration, etc., have been

Received: December 17, 2013
Accepted: February 25, 2014
Published: February 25, 2014

successfully used to obtain well-defined structures of a uniform morphology.[13−16] However, most of these methods generally suffer from either the requirement of bulky and expensive apparatus, laborious operations, or incapability of scalable production, etc.[13−16,23] To meet these formidable challenges, it is strongly desired to develop a cost-effective, facile, scalable method to fulfill the morphology purification.

Among various advanced functional materials of morphology-sensitive uses, catalysts of a unique shape have received particular attention.[1,2,5−8] In the frontier area of advanced catalysts, numerous efforts have been devoted to develop high-performance photocatalysts for environmental issues, especially for photodegradation of organic pollutants.[31−40] While the traditional semiconductor-based photocatalysts have witnessed a tremendous development in this direction,[33,34] the inauguration of new-type catalytic species has currently been considered to be an important issue to achieve high-quality photocatalysts,[31,32,35−39,41−46] wherein those based on silver halide (AgX, where X = Cl, Br, I) have recently gained much attention.[11,47−64] This is due to their outstanding visible-light-driven catalytic reactivity. Nevertheless, despite the numerous successes in enhancing their catalytic reactivity, their unsatisfactory durability is a tough challenge that is encountered by scientists.

To tackle these challenges, we report herein our new findings that AgI-based photocatalysts of distinct morphologies, to say, ill-defined irregular AgI structures, or their mixture with towerlike structures, could be fabricated by a precipitation reaction between $AgNO_3$ and KI. Compared to the former, the mixed structures display superior catalytic reactivity toward the photodegradation of Methyl Orange (MO) pollutant under visible-light or sunlight irradiations. However, they unfortunately exhibit poor catalytic durability. Interestingly, we showed that AgI of a well-defined yet uniform towerlike morphology could be facilely produced after the mixed structures were immersed in a KI aqueous solution under ambient conditions. More excitingly, a boosted catalytic durability and an enhanced catalytic reactivity were achieved simultaneously after such simple morphology purification, wherein the catalytic reactivity of our towerlike AgI displayed only slight fluctuations after the catalytic reactions were performed 20 times continuously and consecutively.

The significance of our investigation is two-fold. First, considering the diversity of the microstructures/nanostructures and their multifunctionality, our morphology purification protocol in terms of a simple chemical dissolution might be extended to some other microsystems/nanosystems, wherein advanced functional materials of a well-defined uniform morphology and desired functions might be easily produced in a large scale. Second, but not least, taking into account the general concerns of catalysts, our work might initiate new and varied ideal for high-quality catalysts of a boosted durability and catalytic reactivity, which are subjects of paramount importance in modern materials science.

2. MATERIALS AND METHODS

2.1. Materials. Silver nitrate ($AgNO_3$, Alfa Aesar, >99.9%), potassium iodide (KI, Sinopharm Chemical Reagent Co., Ltd., >99.0%,), and Methyl Orange (MO, Alfa Aesar, >98%) were used as received, without additional treatment.

2.2. Synthesis of AgI-Based Structures. In a typical synthesis process, a 2.4 mL aqueous solution of $AgNO_3$ (0.5 M) was added dropwise into a 20 mL aqueous solution of KI (0.05 M) within ca. 4 min at room temperature under vigorous magnetic stirring. An opaque dispersion with a yellowish color was obtained immediately after the addition of $AgNO_3$. Subsequently, the stirring was continuously maintained for another 20 min. The resultant precipitates were collected and washed thoroughly with ultrapure Milli-Q water via repeating centrifugation (8000 rpm, 5 min). For the synthesis of the mixture of irregular and towerlike AgI structures, almost similar operations were carried out, except that a 0.8 mL aqueous solution of $AgNO_3$ was used.

2.3. Morphology Purification via a KI-Assisted Chemical Dissolution. The mixture of the as-fabricated irregular and towerlike AgI structures (800 mg) was dispersed into an aqueous solution of KI (0.5 M 400 mL) at room temperature under vigorous stirring. The stirring was continuously maintained for 30 min, after which the products were collected and washed thoroughly with ultrapure Milli-Q water by means of repeating centrifugation (8000 rpm, 5 min). Yellowish solids of *ca.* 520 mg were obtained.

2.4. Photocatalytic Experiments. For the photocatalytic experiments driven by visible-light irradiation, our AgI structures (40 mg) were dispersed in a 6 mL aqueous solution of Methyl Orange (MO, 15 mg L^{-1}), wherein a quartz cuvette was used as the reactor. A 500-W xenon arc lamp installed in a laboratory lamp housing system (CHF-XM35-500 W, Beijing Trusttech Co., Ltd., China) was employed as the light source. The light passed through a 10-cm water filter and a UV cutoff filter (>400 nm) before entering the reactor. The reaction system was kept for 30 min in a darkroom to achieve an equilibrium adsorption state before visible-light irradiation. During the reaction, aliquot of the dispersion (250 μL) was taken out from the system for real-time sampling. The degradation reaction was monitored by measuring the real-time UV-vis absorption of MO at 463 nm. For the evaluation of the catalytic activities, C is the concentration of MO at a real-time t, and C_0 is the concentration of the MO solution immediately before it was kept in darkness. The rate constant of the reaction was deduced by a kinetic linear simulation of the experimental result.

In the cases of the catalytic reactions driven by sunlight irradiation, almost similar experimental conditions were applied, except that the reaction systems were irradiated directly by sunlight. Practically, these experiments were operated at the same time and in the same place with the same sunlight intensity (ca. 50 mW cm^{-2}) to make the data reasonably comparable. In these cases, the recycling experiments could be carried out only when the weather conditions permit sunlight of the same intensity.

2.5. Apparatus, Characterizations, and Measurements. The scanning electron microscopy (SEM) measurements were carried out on a Hitachi Model S-4800 system, wherein an accelerating voltage of 10 kV was employed. The energy-dispersive X-ray spectroscopy (EDX) was measured with a Horiba Model EMAX X-act energy-dispersive spectroscopy device that was attached to the Hitachi Model S-4800 system. In this case, an accelerating voltage of 15 kV was employed. X-ray photoelectron spectroscopy (XPS) was performed on a VG Scientific Model ESCALab220i-XL electron spectrometer using 300 W Al Kα radiation. The binding energies were referenced to the C 1s line at 284.8 eV from adventitious carbon. X-ray diffraction (XRD) measurements were performed on a PANalytical X'Pert PRO instrument with Cu Kα radiation. UV-vis diffuse reflectance

spectra were obtained on an UV-vis spectrophotometer (Hitachi, Model U-3900) using $BaSO_4$ as references. The MO degradation was monitored using a Hitachi U-3900 spectrophotometer. The specific surface areas of our AgI-based structures were measured by means of nitrogen gas adsorption at −196 °C using a TriStar II 3020 (Micromeritics, USA) after the samples were degassed under vacuum at 120 °C overnight, and the specific surface areas were estimated in terms of the Brunauer−Emmett−Teller (BET) method. All the measurements and experiments were carried out at ambient temperature except where noted.

3. RESULTS AND DISCUSSION

3.1. Fabrication and Characterization of the AgI Structures. As illustrated in Figure 1A, for a typical fabrication,

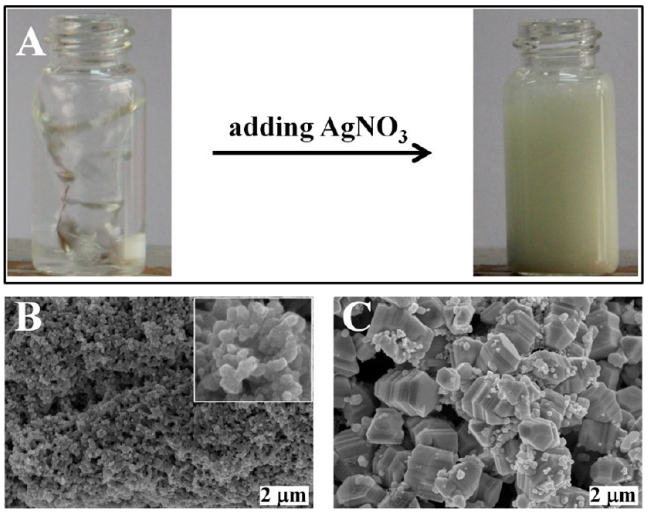

Figure 1. (A) Photographs for the fabrication of AgI structures. (B) Scanning electron microscopy (SEM) image of the irregular AgI structures. [Inset in panel (B) shows a high-magnification SEM image.] (C) SEM image of the mixed structures.

an $AgNO_3$ aqueous solution was added dropwise into a KI aqueous solution under vigorous stirring at room temperature. A yellowish opaque dispersion was obtained immediately after the addition of $AgNO_3$. The stirring was maintained for 20 min, after which the products were collected by centrifugation and washed thoroughly with ultrapure Milli-Q water. As shown in Figure 1B, ill-defined irregular structures with an averaged size of ca. 150 nm were produced when 2.4 mL of $AgNO_3$ solution was used. In contrast, big microstructures of a towerlike morphology, with an average size of ca. 1.9 μm, accompanied by numerous irregular species (Figure 1C), were obtained when the volume of the $AgNO_3$ solution was decreased by a factor of 3.

The components of our products were investigated by energy-dispersive X-ray spectroscopy (EDX) analysis. As shown in Figure S1A in the Supporting Information, for the irregular structures, silver (Ag) and iodide (I) elements could be detected evidently, wherein a semiquantitative analysis shows that the atomic ratio between Ag and I is ~50:50. This datum is almost similar to the theoretic stoichiometric atomic ratio between Ag and I species of AgI, which should be 1:1. In the case of the mixed structures, almost similar results are obtained (see Figure S1B in the Supporting Information). These facts indicate the formation of the AgI species. To verify this, our samples are further characterized by X-ray photoelectron spectroscopy (XPS), as shown in Figure 2 and Figure S2 in

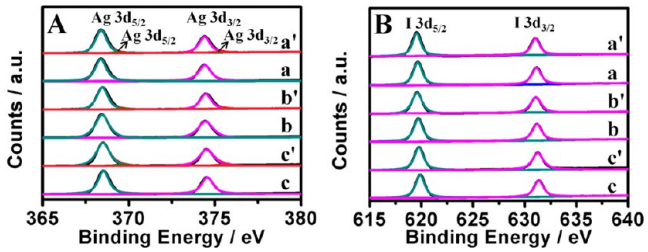

Figure 2. XPS spectra of (A) Ag 3d and (B) I 3d of the irregular (spectrum a), mixed (spectrum b), and towerlike (spectrum c) structures before the catalytic reactions. Those of the corresponding samples after the catalytic reactions are repeated three times (spectra a′, b′, and c′, respectively) are also shown for comparison. For more-detailed information, see Figure S2 in the Supporting Information.

the Supporting Information. It can be seen that two bands at ca. 368.3 and 374.3 eV, which are ascribed to the Ag $3d_{5/2}$ and Ag $3d_{3/2}$ binding energies of the Ag^+ of AgI, respectively, could be observed.[65−67] On the other hand, two bands at ca. 619.5 and 631.2 eV, which are attributed to the I $3d_{3/2}$ and I $3d_{5/2}$ binding energies of the I^- species of AgI, could also be observed.[66,67] From these XPS spectra, the mole ratio between Ag^+ and I^- species could be semiquantitatively estimated to be ~1:1. Together with the results of EDX investigations (Figure S1 in the Supporting Information), these facts further verify the formation of AgI.

The X-ray diffraction (XRD) pattern of our samples was investigated to identify the formation of AgI species. As shown in Figure 3 (spectrum a), the irregular species display distinct

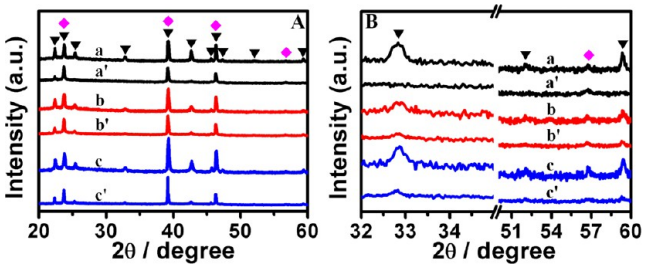

Figure 3. (A) XRD pattern of the irregular (spectrum a), mixed (spectrum b), and towerlike (spectrum c) structures before the catalytic reactions. Those of the corresponding samples after the catalytic reactions are repeated three times (spectra a′, b′, and c′, respectively) are also shown for comparison. (B) Enlarged XRD pattern of the corresponding samples in the 2θ ranges of 32°−35° and 50°−60°. The diffraction peaks ascribing to β-AgI and γ-AgI are denoted by a black solid inverted triangle (▼) and a magenta solid diamond-shaped symbol (◆), respectively.

diffraction peaks (2θ) at 22.3°, 25.3°, 32.8°, 42.6°, 45.6°, 47.2°, 52.0°, and 59.3°, which could be indexed to the characteristic (100), (101), (102), (103), (200), (201), (202), and (203) planes of the typical hexagonal (β-AgI) phase (JCPDS File Card No. 09-0374), respectively.[64,66,67] Besides, three diffraction peaks at 23.7°, 39.2°, and 46.3°, which could either be attributed to the (002), (110), and (112) planes of β-AgI, or the (111), (220), and (311) planes of γ-AgI (JCPDS File Card No. 09-0399),[68] respectively, could also be observed. Note that it is difficult to assign this set of peaks exactly to β-AgI or γ-AgI,

because of their extremely close reflection position.[69] Nevertheless, a diffraction peak at 56.7°, ascribing to the (400) plane of γ-AgI, could be observed. For the XRD pattern of the mixed structures, almost similar results are obtained, as shown in Figure 3 (spectrum b). These facts indicate the coexistence of of β-AgI and γ-AgI phases in the as-fabricated structures. This is similar to the reports of others, where it is suggested that the AgI species are usually a symbiont of β-AgI and γ-AgI.[69,70]

For visible-light-driven photocatalysts, it is required that they should be visible-light active to achieve an efficient energy supply. The UV-vis diffuse reflectance spectra of our structures are illustrated in Figure 4A. It can be seen that the samples

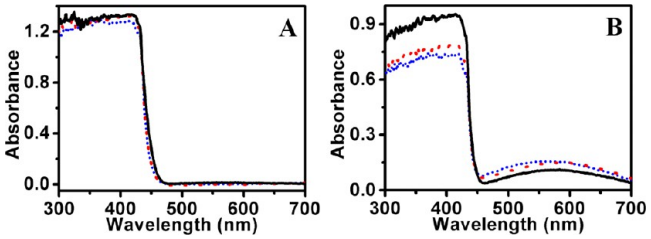

Figure 4. UV-vis diffuse reflectance spectra of (A) the irregular (black, solid line), mixed (red, dotted line), and towerlike structures (blue, short dotted line) before the catalytic reactions and (B) the corresponding samples after the catalytic reactions have been repeated three times.

display distinct absorption in the UV region with their absorption edge extended to ca. 465 nm, which is located in visible region.[66] This result indicates that our AgI might be catalytically active under visible-light irradiation.

3.2. Photocatalytic Performance of the Irregular and Mixed Structures under Visible-Light Irradiation. As shown in Figure 5A, the photocatalytic reactivity of our AgI

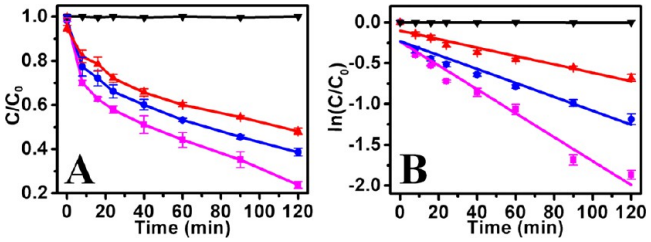

Figure 5. (A) Photocatalytic performances and (B) the corresponding kinetic linear simulation curves of our photocatalysts toward MO degradation under visible-light irradiation. The catalysts are the (▲) irregular, (●) mixed, and (■) towerlike structures, respectively. The result obtained from a blank experiment (denoted by a solid inverted triangle (▼)) is also presented for comparison.

structures was investigated in terms of MO photodegradation under visible-light irradiation. The reaction process was monitored by means of measuring the real-time UV-vis spectra of MO at 463 nm. Experimentally, prior to the light irradiation, a dark adsorption was performed to achieve an equilibrium adsorption state. As shown in Figure 5A (black curve), when no catalysts are used, negligible MO degradation could be observed, indicating that the self-photosensitized MO decomposition under our experimental conditions could basically be ignored. On the other hand, when our irregular AgI species are involved in the reaction system, ca. 50% MO molecules are decomposed within 120 min. This suggests that our AgI could indeed work as visible-light-driven photocatalysts for the MO degradation. In contrast, when the mixed structures are used, almost 60% of the MO molecules are decomposed under similar conditions. As plotted in Figure 5B, there is a nice linear correlation between $\ln(C/C_0)$ and the reaction time (t), indicating that the MO decomposition over our catalysts follows the first-order kinetics. The rate constant of the catalytic reaction over the irregular structures is estimated to be 0.005 min^{-1}, while that over the mixed structures is ca. 0.009 min^{-1}. These results indicate that compared to the irregular AgI species, our mixed structures could display enhanced catalytic reactivity.

The specific surface areas of our AgI structures were estimated via BET method. The results show that the BET surface area of our irregular structures is ca. 0.58 $m^2\ g^{-1}$, while that of our mixed structures is ca. 0.53 $m^2\ g^{-1}$. These results are very close to those of the AgX-based catalysts (X = Br, Cl, PO_4) reported previously,[62,71] indicating that the boosted catalytic reactivity might be attributed to reasons other than their specific surface areas. The superior catalytic reactivity of a catalyst of a unique yet well-defined architecture could be partially attributed to the existence of high-density catalytically active sites, such as corners, edges, tips and steps, etc.[1,2,5,8,72] As suggested by the SEM images of our samples (Figures 1A and 1B), compared to the irregular structures, there exist more corners, steps, and edges in our towerlike architectures. We thus suggest that the enhanced catalytic reactivity might partially be attributed to this issue.

Besides, it is widely known that morphology-sensitive catalytic activity could also be understood in terms of the different reaction performances induced by specific crystal facets selectively exposed by anisotropic structures.[1,2,5,8,72] As discussed above by the XRD pattern (Figure 3, spectra a and b), our AgI structures are a symbiont of β-AgI and γ-AgI. On one hand, the peak at ca. 39.2° and 23.7° could be attributed to the (110) and (002) facets of β-AgI, respectively. In this case, the ratios between (110) and (002), estimated using the latter as a reference (that is, 100), are ca. 163.9 and 202.8 for the irregular and mixed structures, respectively. For the standard JCPDS file of β-AgI, this ratio is generally ca. 85.0, which is smaller than the corresponding data for our AgI. Meanwhile, it can be seen that an increasing tendency could be observed from these data when our AgI is changed from the irregular to the mixed structures. On the other hand, as discussed above, these two peaks at ca. 39.2° and 23.7° could also be indexed to the (220) and (111) facets of γ-AgI, respectively. In this case, similar comparison results, estimated using the (111) facet of γ-AgI as a reference, are obtained. These facts indicate that compared to the irregular AgI structures, the towerlike counterparts are enriched with (110) facets of either β-AgI or γ-AgI. We accordingly suggest that the relative enrichment of (110) facets in our towerlike structures might also contribute partially to the superior catalytic reactivity of our mixed structures.

Practically, in addition to a high catalytic reactivity, durability is another critical criterion that is required by high-quality photocatalysts of potential applications. The catalytic durability of the mixed structures was evaluated by performing the MO degradation reactions repeatedly several times. As shown in Figure 6A, we unfortunately find that their catalytic reactivity exhibits distinct decrease under visible-light irradiation after the reactions are repeated only three times continuously. These results indicate that our mixed structures could not work as

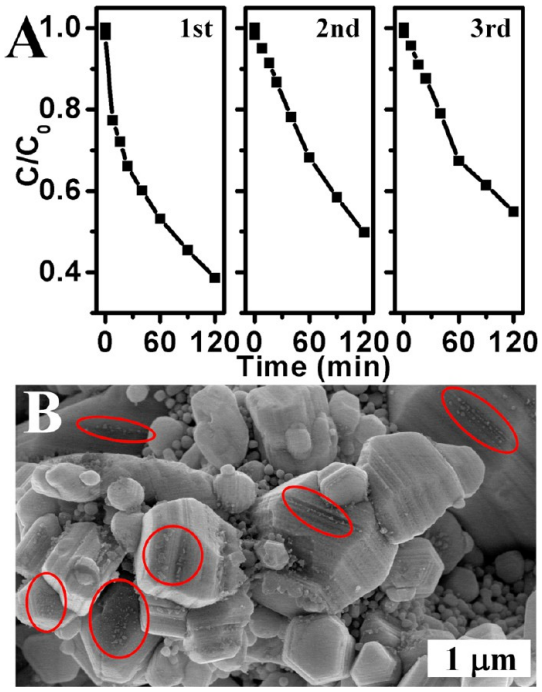

Figure 6. (A) Three consecutive cycling curves of MO degradation over the mixed AgI structures under visible-light irradiation. (B) Typical SEM image of the mixed structures measured after the catalytic reactions have been repeated three times. The tiny species appeared on the surfaces, corners, edges, or steps of the towerlike structures after the catalytic reactions are indicated by circles.

stable catalysts for the bleaching of organic pollutants, although compared to the irregular AgI structures they could display high catalytic reactivity. As shown in Figure 6B, the SEM image of the mixed structures after the catalytic reactions was investigated. It can be seen that compared to that before the catalytic reactions (Figure 1C), numerous tiny species are observed from the surfaces, corners, edges, or steps of the towerlike structures. More importantly, we note that the basic morphology of the towerlike AgI displays negligible changes. These observations imply that our towerlike AgI structures themselves might be stable species, and that the observed tiny species might come from the irregular AgI structures but not be generated by the towerlike AgI achitectures during the catalytic reactions. We thus suggest that the deactivated catalytic reactivity during the recyclings could be tentatively attributed to the loss of some of the catalytically active sites, which are screened by the tiny species that come from the irregular AgI.

3.3. Morphology Purification via a KI-assisted Chemical Dissolution and the Photocatalytic Reactivity of the Towerlike Structures. Based on these primary understandings and analyses, it could be proposed that high-quality AgI-based photocatalysts simultaneously featured with an enhanced catalytic durability and reactivity would be realized if AgI species of a uniform towerlike morphology could be obtained. Along this line of thought, we attempted to separate the irregular and towerlike structures via centrifugation. Unfortunately, the results show that these two structures of different size and morphology could not be separated very well (see Figure S3 in the Supporting Information). As it is widely known that the AgI solids could readily dissolve in a concentrated KI aqueous solution in terms of a surface chemical reaction, mAgI (solid) + nKI (aqueous solution) = $K_n[Ag_mI_{(n+m)}]$ (aqueous solution), producing water-soluble $K_n[Ag_mI_{(n+m)}]$ species.[73,74] On the other hand, it has been verified that compared to that occurs on a smooth surface of a larger structure, the solid–liquid surface reaction occurs more rapidly on a smaller structure of an irregular surface.[75−79] According to the Noyes–Whitney principle,[75] this is due to the fact that smaller particles provide a larger contact surface for the occurrence of solid–liquid reactions, leading to a preferential chemical dissolution of smaller species.[75−79]

It thus is reasonable to propose that AgI structures of a uniform towerlike morphology might be selectively obtained by immersing our mixed structures in a concentrated KI aqueous solution, since compared to the irregular structures, our towerlike structures exhibit a bigger size and a more smooth surface, as shown in Figures 1B and 1C. Experimentally, to achieve this, 800 mg of the mixed structures were immersed in 400 mL of concentrated KI aqueous solution under ambient conditions. After 30 min, the products were collected by centrifugation and washed thoroughly with ultrapure Milli-Q water. It is found that the amount of the product is decreased to ca. 520 mg after such simple post-treatment, indicating the successful removal of some of the AgI species (yield: 65%). As indicate by the XRD pattern shown in Figure 3 (spectrum c), compared to that of the irregular and mixed structures (Figure 3, spectra a and b), the ratio between the peaks at ca. 39.2° and 23.7° (either indexed to the (110) and (002) facets of β-AgI, or to the (220) and (111) planes of γ-AgI, respectively) of thus-produced samples further increases to 239.9°. Together with the above discussions on the XRD data, this result suggest that the structures removed by our KI-assisted chemical dissolution protocol might be the irregular species, leaving us mainly with towerlike architectures. To confirm this, the SEM images of the products were measured. As shown in Figures 7A and 7B, it is very exciting to find that thus post-treated samples manifest themselves with a uniform morphology of well-defined tower-like structure, wherein negligible irregular species could be observed. This result verifies that a morphology purification could indeed be realized by means of a size- and morphology-selective chemical dissolution.

The catalytic reactivity of such AgI structures of a uniform towerlike morphology were investigated. As shown in Figure 5A, nearly 80% MO molecules are decomposed within 120 min, wherein a rate constant of ca. 0.015 min^{-1} could be derived (Figure 5B). This value is distinctly larger than that of the irregular AgI (0.005 min^{-1}) and that of the mixed structures (0.009 min^{-1}). The durability of our towerlike AgI-based catalysts was also evaluated in terms of performing the bleaching reactions repeatedly. As shown in Figure 7C, the catalytic reactivity display only trivial fluctuations under visible-light irradiation even after the reactions are repeated 20 times continuously and consecutively. Compared to what observed from the mixed structures (Figure 6A), these results strongly indicate that high quality AgI-based catalysts simultaneously featured with a boosted durability and an enchanced catalytic reactivity could be achieved simply by a morphology purification.

As shown in Figure 8, different from that of the mixed structures (Figure 6B), the SEM image of our AgI of a uniform towerlike morphology exhibits only negligible changes after the catalytic reactions are repeated three times, wherein only negligible tiny species could be observed from their surfaces, corners, edges, or steps. These observations solidly confirm that the tiny species appeared on the towerlike architectures of the

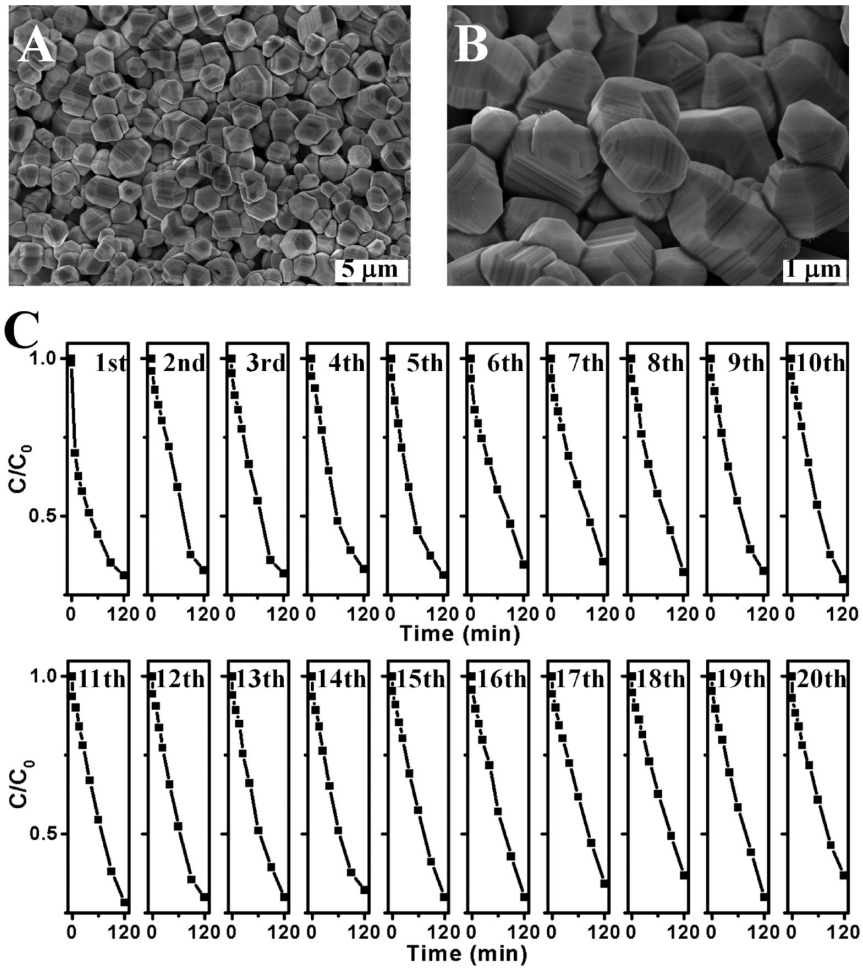

Figure 7. Typical SEM images ((A) low-magnification and (B) high-magnification) of the AgI of a uniform towerlike morphology, which are obtained by a KI-assisted chemical dissolution protocol. (C) Twenty (20) consecutive cycling degradation curves of MO over our towerlike AgI under visible-light irradiation.

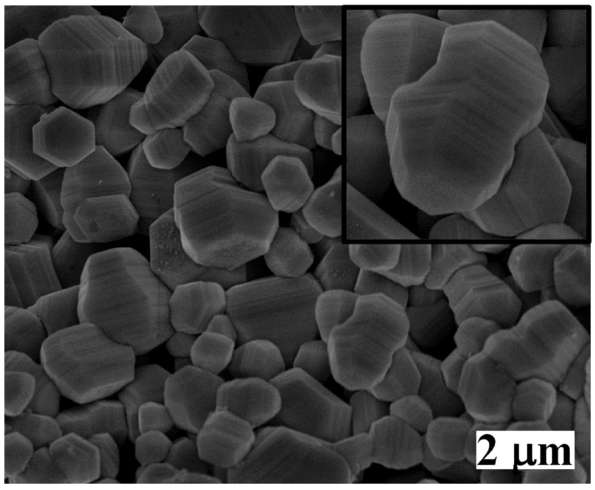

Figure 8. Typical low-magnification and high-magnification SEM (inset) images of the AgI of a uniform towerlike morphology measured after the catalytic reactions have been repeated three times.

mixed structures mainly come from the irregular AgI species but not generated by the towerlike species themselves. It also verifies that compared to the AgI species of an irregular morphology, our towerlike AgI species are, indeed, more-stable architectures. This could be further confirmed by the XRD pattern (Figure 3, spectra a and a′), wherein the diffraction peaks of the irregular AgI structures at ca. 25.3°, 32.8°, 42.6° (which are attributed to the (101), (102), (103) facets of β-AgI, respectively), almost disappeared totally after the catalytic reactions were performed three times. Comparatively, in the cases of the mixed and towerlike structures, these diffractions could still be discerned evidently, although their relative intensity displays decrease somewhat. These XRD facts further confirm that our towerlike AgI architectures are more stable than the irregular structures.

Generally, it is widely known that plain silver halide AgX (X = Cl, Br, and I) are conventionally photosensitive materials, which would be photodecomposed into metallic Ag^0 species under light irradiation. On the other hand, it has recently been proved that the appearance of the artificially or naturally generated plasmonic metallic Ag^0 on the AgX speices before or during the photocatalytic reactions, namely, the formation of Ag/AgX composites, could, in turn, endow these systems with a so-called "self-stability".[54] In this issue, the ex situ or in situ generation of plasmonic metallic Ag^0 species plays a critical role, wherein the photogenerated electrons originally should be captured by Ag^+ would now be captured by O_2 via the metallic Ag^0 formed at the initial stage of the light irradiation. This leads to the formation of photostable Ag/AgX composites.[54] The in

dx.doi.org/10.1021/am405816p | ACS Appl. Mater. Interfaces 2014, 6, 4160−4169

situ generation of plasmonic Ag^0 species in our present case could be verified by the UV-vis diffuse reflectance spectra measured after the photocatalytic reactions. As shown in Figure 4B, compared with those of the samples before the catalytic reactions, broad and strong absorptions around 450−700 nm could also be observed. This result indicates an in situ generation of metallic Ag^0 species during the photocatalytic reactions, which could arouse plasmonic absorptions in the visible region, and meanwhile it suggests the formation of Ag/AgI composites.[47−51,54]

To further verify this proposal experimentally, the samples after the photocatalytic reactions were investigated by EDX analyses, as shown in Figure S4 in the Supporting Information. In these cases, the semiquantitative analyses indicate that the atomic ratio between elemental silver and iodide (Ag/I) is ∼51:49. This value is higher than that of the samples estimated before the photocatalytic reactions, which is very close to ca. 50:50 (see Figure S1 in the Supporting Information). This fact is in accordance with the information deduced from the UV-vis diffuse reflectance spectral analyses (see Figure 4B), further suggesting an in situ generation of metallic Ag^0 species during the photocatalytic reactions. Based on the EDX analyses, the mole ratio between the Ag^0 and Ag^+ could be calculated to be ca. 2:49. To further confirm the in situ generation of metallic Ag^0 species, the XPS spectra of our samples after the photocatalytic reactions were investigated. As shown in Figure 2 and Figure S2 in the Supporting Information, it can be seen that compared to those measured before the catalytic reactions, the XPS spectra of the samples obtained after the catalytic reactions display almost similar spectral profile, except that two bands around 369.3 and 375.1 eV, which could be attributed to the Ag $3d_{5/2}$ and Ag $3d_{3/2}$ binding energies of the metallic Ag^0 species,[48,65] respectively, could be observed via a deconvolution of the silver-related bands (for more-detailed spectra, see Figure S2 in the Supporting Information). Based on the obtained XPS analyses, the surface mole ratio between Ag^0 and Ag^+ is semiquantitatively estimated to be ∼2:49, which is very close to that obtained from the EDX analyses (see Figure S4 in the Supporting Information). Together with the facts derived from the UV-visible diffuse reflectance spectra (Figure 4B) and EDX analyses (Figure S4 in the Supporting Information), these results further verify the photoinduced generation of metallic Ag^0 species in our samples during the catalytic reactions.

Note that no distinct diffraction peaks hat are ascribed to the metallic Ag^0 could be observed from the XRD pattern of our samples measured after the catalytic reactions (Figure 3, spectra a′, b′, and c′). This observation is similar to that reported by others, wherein the possible reason could be attributed to the limited amount of Ag^0, their small particle size, and their high dispersion in the composite as well.[53,54] Nevertheless, the experimental results of the UV-vis diffuse reflectance spectra (Figure 4B), EDX analyses (Figure S4 in the Supporting Information), and XPS spectra (Figure 2 and Figure S2 in the Supporting Information) strongly imply an in situ photoinduced generation of Ag^0 in our AgI, leading to the formation of the Ag/AgI species. Based on the above-mentioned facts, it could be suggested that it is the synergistic effect of the morphology purification and the metallic Ag^0-promoted self-stabilization[54] that contributes much for the boosted catalytic durability and the enhanced catalytic reactivity of the structures of a uniform towerlike morphology.

Practically, considering the energy savings and utilization, sunlight, which is the most economical and renewable energy source, should be the most attractive candidate to supply energy for the operation of photocatalysts.[31,32] The catalytic reactivity of our catalysts are also evaluated in terms of MO degradation under sunlight irradiation. It should be pointed out that these experiments were carried out at the same time and the same place with the same sunlight intensity, to make the data reasonably comparable. As shown in Figures 9A and 9B,

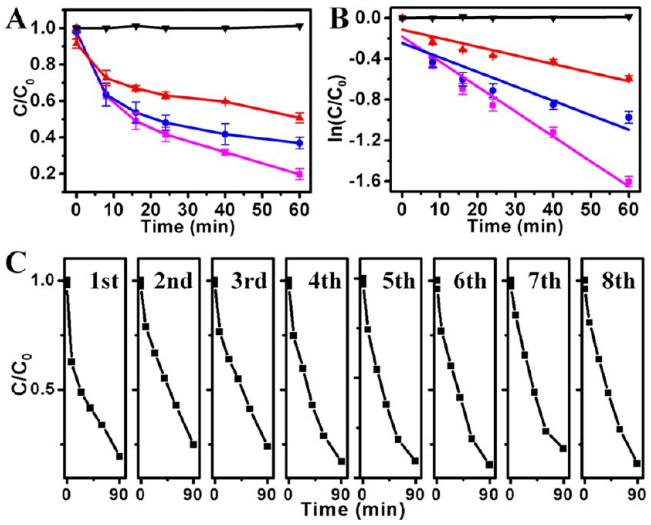

Figure 9. (A) Photocatalytic performances and (B) the corresponding kinetic linear simulation curves of our photocatalysts toward the MO degradation under sunlight irradiation. The catalysts used are the irregular AgI (denoted by a solid triangle, ▲), the mixed structure (denoted by a solid circle, ●), and the towerlike structure (denoted by a solid square, ■), respectively. The result obtained from a blank experiment (denoted by a solid inverted triangle, ▼) is also presented for comparison. (C) Eight consecutive cycling degradation curves of MO over our towerlike AgI under sunlight irradiation.

compared to the irregular and the mixed structures, our AgI architectures of a uniform towerlike morphology display an enhanced catalytic reactivity. This tendency is similar to that obtained when our catalytic reactions are energized by visible-light irradiation (Figure 5). The durability of our catalysts of a uniform towerlike morphology under the sunlight irradiation was also evaluated by performing the MO degradation reactions repeatedly several times. As shown in Figure 9C, it is found that the catalytic reactivity displays only slight fluctuation under sunlight irradiation after the reactions are operated eight times continuously. Experimentally, such recycling operations were only carried out eight times, since it is not so easy to choose appropriate weather conditions of the same sunlight intensity, for a reasonable comparison. Nevertheless, these results suggest that our AgI-base catalysts of a uniform towerlike morphology could be used as high-quality visible-light/sunlight-driven photocatalysts for a bleaching of organic pollutants, indicating their bright future for potential applications.

4. CONCLUSIONS

In summary, we herein report that AgI species of different morphologies, namely irregular structures, and their mixture with tower-like architectures, could be formulated by a precipitation reaction between $AgNO_3$ and KI. Compared to the irregular structures, the mixture displays enhanced catalytic reactivity toward MO degradation under visible-light/sunlight irradiations. However, they display poor catalytic durability.

Interestingly, in terms of a KI-assisted chemical dissolution, the irregular structures could be easily removed from the mixture, producing AgI architectures of a well-defined yet uniform towerlike morphology. More excitingly, compared to the mixed structures, our towerlike architectures of a uniform morphology display not only a boosted durability but also an enhanced catalytic reactivity, indicating their bright future as high-quality catalysts of potential uses. On one hand, in terms of a simple morphology purification, our investigation likely provides new ideal for the achievement of excellent catalysts simultaneously featured with high durability and superior catalytic reactivity. On the other front, considering the rich diversity of the microstructures/nanostructures and their multifunctionality, our chemical dissolution-based morphology purification protocol might be extended to other systems. This will endow researchers with new and varied opportunities for various well-defined structures of a uniform morphology, wherein advanced functional materials of desirable properties and functions might be developed.

■ ASSOCIATED CONTENT

Ⓢ Supporting Information

EDX elemental analyses of our AgI species, XPS spectra of Ag 3d of our samples, SEM images of the mixed structures measured after a centrifugation-based morphology purification. This material is available free of charge via the Internet at http://pubs.acs.org.

■ AUTHOR INFORMATION

Corresponding Authors

*Tel.: (+) 86-10-82615803. Fax: (+) 86-10-62569564. E-mails: chenpl@iccas.ac.cn, cpl@zzu.edu.cn.

*Tel.: (+) 86-371-67781556. Fax: (+) 86-371-67766667. E-mail: lts34@zzu.edu.cn.

*Tel.: (+) 86-10-82615803. Fax: (+) 86-10-62569564. E-mail: liumh@iccas.ac.cn.

Notes

The authors declare no competing financial interest.

■ ACKNOWLEDGMENTS

This work was supported financially by the National Natural Science Foundation of China (Nos. 21372225, 21321063, and 91027042), the National Key Basic Research Project of China (Nos. 2011CB932301 and 2013CB834504), and the Chinese Academy of Sciences (Nos. XDA09030200 and 1731300500015). The authors are grateful to Prof. Guangtao Li from the Department of Chemistry, Tsinghua University for great helps in the measurement of the BET surface areas of the structures.

■ REFERENCES

(1) Zhou, K.; Li, Y. Catalysis Based on Nanocrystals with Well-Defined Facets. *Angew. Chem., Int. Ed.* **2012**, *51*, 602−613.

(2) Wang, D.; Xie, T.; Li, Y. Nanocrystals: Solution-Based Synthesis and Applications as Nanocatalysts. *Nano Res.* **2009**, *2*, 30−46.

(3) Ray, P. C. Size and Shape Dependent Second Order Nonlinear Optical Properties of Nanomaterials and Their Application in Biological and Chemical Sensing. *Chem. Rev.* **2010**, *110*, 5332−5365.

(4) Xu, S.; Wang, Z. L. One-Dimensional ZnO Nanostructures: Solution Growth and Functional Properties. *Nano Res.* **2011**, *4*, 1013−1098.

(5) Xiao, J.; Qi, L. Surfactant-Assisted, Shape-Controlled Synthesis of Gold Nanocrystals. *Nanoscale* **2011**, *3*, 1383−1396.

(6) Jiang, P.; Zhou, J.-J.; Fang, H.-F.; Wang, C.-Y.; Wang, Z. L.; Xie, S.-S. Hierarchical Shelled ZnO Structures Made of Bunched Nanowire Arrays. *Adv. Funct. Mater.* **2007**, *17*, 1303−1310.

(7) An, K.; Somorjai, G. A. Size and Shape Control of Metal Nanoparticles for Reaction Selectivity in Catalysis. *ChemCatChem* **2012**, *4*, 1512−1524.

(8) Zhou, Z.-Y.; Tian, N.; Li, J.-T.; Broadwell, I.; Sun, S.-G. Nanomaterials of High Surface Energy with Exceptional Properties in Catalysis and Energy Storage. *Chem. Soc. Rev.* **2011**, *40*, 4167−4185.

(9) Talapin, D. V.; Lee, J.-S.; Kovalenko, M. V.; Shevchenko, E. V. Prospects of Colloidal Nanocrystals for Electronic and Optoelectronic Applications. *Chem. Rev.* **2010**, *110*, 389−458.

(10) Wang, H.; Qi, L. Controlled Synthesis of Ag_2S, Ag_2Se, and Ag Nanofibers by Using a General Sacrificial Template and Their Application in Electronic Device Fabrication. *Adv. Funct. Mater.* **2008**, *18*, 1249−1256.

(11) Ai, K.; Liu, Y.; Ruan, C.; Lu, L.; Lu, G. sp^2 C-Dominant N-Doped Carbon Sub-micrometer Spheres with a Tunable Size: A Versatile Platform for Highly Efficient Oxygen-Reduction Catalysts. *Adv. Mater.* **2013**, *25*, 998−1003.

(12) Luo, B.; Wang, B.; Liang, M.; Ning, J.; Li, X.; Zhi, L. Reduced Graphene Oxide-Mediated Growth of Uniform Tin−Core/Carbon-Sheath Coaxial Nanocables with Enhanced Lithium Ion Storage Properties. *Adv. Mater.* **2012**, *24*, 1405−1409.

(13) Kowalczyk, B.; Lagzi, I.; Grzybowski, B. A. Nanoseparations: Strategies for Size and/or Shape-Selective Purification of Nanoparticles. *Curr. Opin. Colloid Interface Sci.* **2011**, *16*, 135−148.

(14) Wu, W.; Huang, J.; Wu, L.; Sun, D.; Lin, L.; Zhou, Y.; Wang, H.; Li, Q. Two-step Size- and Shape-Separation of Biosynthesized Gold Nanoparticles. *Sep. Purif. Technol.* **2013**, *106*, 117−122.

(15) Liu, J.-F.; Yu, S.-J.; Yin, Y.-G.; Chao, J.-B. Methods for Separation, Identification, Characterization and Quantification of Silver Nanoparticles. *Trends Anal. Chem.* **2012**, *33*, 95−106.

(16) Buck, M. R.; Schaak, R. E. Emerging Strategies for the Total Synthesis of Inorganic Nanostructures. *Angew. Chem., Int. Ed.* **2013**, *52*, 6154−6178.

(17) Kang, Y.; Li, M.; Cai, Y.; Cargnello, M.; Diaz, R. E.; Gordon, T. R.; Wieder, N. L.; Adzic, R. R.; Gorte, R. J.; Stach, E. A.; Murray, C. B. Heterogeneous Catalysts Need Not Be so "Heterogeneous": Monodisperse Pt Nanocrystals by Combining Shape-Controlled Synthesis and Purification by Colloidal Recrystallization. *J. Am. Chem. Soc.* **2013**, *135*, 2741−2747.

(18) Schaak, R. E.; Williams, M. E. Full Disclosure: The Practical Side of Nanoscale Total Synthesis. *ACS Nano* **2012**, *6*, 8492−8497.

(19) Ma, X.; Kuang, Y.; Bai, L.; Chang, Z.; Wang, F.; Sun, X.; Evans, D. G. Experimental and Mathematical Modeling Studies of the Separation of Zinc Blende and Wurtzite Phases of CdS Nanorods by Density Gradient Ultracentrifugation. *ACS Nano* **2011**, *5*, 3242−3249.

(20) Akbulut, O.; Mace, C. R.; Martinez, R. V.; Kumar, A. A.; Nie, Z.; Patton, M. R.; Whitesides, G. M. Separation of Nanoparticles in Aqueous Multiphase Systems through Centrifugation. *Nano Lett.* **2012**, *12*, 4060−4064.

(21) Bass, J. D.; Ai, X.; Bagabas, A.; Rice, P. M.; Topuria, T.; Scott, J. C.; Alharbi, F. H.; Kim, H.-C.; Song, Q.; Miller, R. D. An Efficient and Low-Cost Method for the Purification of Colloidal Nanoparticles. *Angew. Chem., Int. Ed.* **2011**, *50*, 6538−6542.

(22) Krieg, E.; Weissman, H.; Shirman, E.; Shimoni, E.; Rybtchinski, B. A Recyclable Supramolecular Membrane for Size-Selective Separation of Nanoparticles. *Nat. Nanotechnol.* **2011**, *6*, 141−146.

(23) Lohse, S. E.; Eller, J. R.; Sivapalan, S. T.; Plews, M. R.; Murphy, C. J. A Simple Millifluidic Benchtop Reactor System for the High-Throughput Synthesis and Functionalization of Gold Nanoparticles with Different Sizes and Shapes. *ACS Nano* **2013**, *7*, 4135−4150.

(24) Khanal, B. P.; Zubarev, E. R. Purification of High Aspect Ratio Gold Nanorods: Complete Removal of Platelets. *J. Am. Chem. Soc.* **2008**, *130*, 12634−12635.

(25) Xiong, B.; Cheng, J.; Qiao, Y.; Zhou, R.; He, Y.; Yeung, E. S. Separation of Nanorods by Density Gradient Centrifugation. *J. Chromatogr. A* **2011**, *1218*, 3823−3829.

(26) Steinigeweg, D.; Schütz, M.; Salehi, M.; Schlücker, S. Fast and Cost-Effective Purification of Gold Nanoparticles in the 20−250 nm Size Range by Continuous Density Gradient Centrifugation. *Small* **2011**, *7*, 2443−2448.
(27) Essinger−Hileman, E. R.; Popczun, E. J.; Schaak, R. E. Magnetic Separation of Colloidal Nanoparticle Mixtures Using a Material Specific Peptide. *Chem. Commun.* **2013**, *49*, 5471−5473.
(28) Jiang, Y.; Xu; Wang, C.; Shao, H.; Wang, Z.; Cui, Y. A Novel Separation Technique for Aqueous Nanoparticles Based on a Phase Transfer Approach. *J. Mater. Chem.* **2012**, *22*, 13469−13472.
(29) Sun, Y.; Xia, Y. Shape-Controlled Synthesis of Gold and Silver Nanoparticles. *Science* **2002**, *298*, 2176−2179.
(30) Skrabalak, S. E.; Au, L.; Li, X.; Xia, Y. Facile Synthesis of Ag Nanocubes and Au Nanocages. *Nat. Protoc.* **2007**, *2*, 2182−2190.
(31) Chen, C.; Ma, W.; Zhao, J. Semiconductor-Mediated Photodegradation of Pollutants under Visible-Light Irradiation. *Chem. Soc. Rev.* **2010**, *39*, 4206−4219.
(32) Kubacka, A.; Fernández-García, M.; Colón, G. Advanced Nanoarchitectures for Solar Photocatalytic Applications. *Chem. Rev.* **2012**, *112*, 1555−1614.
(33) Legrini, O.; Oliveros, E.; Braun, A. M. Photochemical Processes for Water Treatment. *Chem. Rev.* **1993**, *93*, 671−698.
(34) Hoffmann, M. R.; Martin, S. T.; Choi, W.; Bahnemannt, D. W. Environmental Applications of Semiconductor Photocatalysis. *Chem. Rev.* **1995**, *95*, 69−96.
(35) Zhang, D.; Li, G.; Yu, J. C. Inorganic Materials for Photocatalytic Water Disinfection. *J. Mater. Chem.* **2010**, *20*, 4529−4536.
(36) Sun, H.; Cao, L.; Lu, L. Magnetite/Reduced Graphene Oxide Nanocomposites: One Step Solvothermal Synthesis and Use as a Novel Platform for Removal of Dye Pollutants. *Nano Res.* **2011**, *4*, 550−562.
(37) Zhou, X.; Lan, J.; Liu, G.; Deng, K.; Yang, Y.; Nie, G.; Yu, J.; Zhi, L. Facet-Mediated Photodegradation of Organic Dye over Hematite Architectures by Visible Light. *Angew. Chem., Int. Ed.* **2012**, *51*, 178−182.
(38) Jiang, J.; Zhao, K.; Xiao, X.; Zhang, L. Synthesis and Facet-Dependent Photoreactivity of BiOCl Single Crystalline Nanosheets. *J. Am. Chem. Soc.* **2012**, *134*, 4473−4476.
(39) Zhao, X.; Jin, W.; Cai, J.; Ye, J.; Li, Z.; Ma, Y.; Xie, J.; Qi, L. Shape- and Size-Controlled Synthesis of Uniform Anatase TiO_2 Nanocuboids Enclosed by Active {100} and {001} Facets. *Adv. Funct. Mater.* **2011**, *21*, 3554−3563.
(40) Cai, J.; Ye, J.; Chen, S.; Zhao, X.; Zhang, D.; Chen, S.; Ma, Y.; Jin, S.; Qi, L. Self-cleaning, Broadband and Quasi-Omnidirectional Antireflective Structures Based on Mesocrystalline Rutile TiO_2 Nanorod Arrays. *Energy Environ. Sci.* **2012**, *5*, 7575−7581.
(41) Zhu, H.; Ke, X.; Yang, X.; Sarina, S.; Liu, H. Reduction of Nitroaromatic Compounds on Supported Gold Nanoparticles by Visible and Ultraviolet Light. *Angew. Chem., Int. Ed.* **2010**, *49*, 9657−9661.
(42) Chen, X.; Zheng, Z.; Ke, X.; Jaatinen, E.; Xie, T.; Wang, D.; Guo, C.; Zhao, J.; Zhu, H. Supported Silver Nanoparticles as Photocatalysts under Ultraviolet and Visible Light Irradiation. *Green Chem.* **2010**, *12*, 414−419.
(43) Chen, X.; Zhu, H.-Y.; Zhao, J.-C.; Zheng, Z.-F.; Gao, X.-P. Visible-Light-Driven Oxidation of Organic Contaminants in Air with Gold Nanoparticle Catalysts on Oxide Supports. *Angew. Chem., Int. Ed.* **2008**, *47*, 5353−5356.
(44) Sarina, S.; Waclawik, E. R.; Zhu, H. Photocatalysis on Supported Gold and Silver Nanoparticles under Ultraviolet and Visible Light Irradiation. *Green Chem.* **2013**, *15*, 1814−1833.
(45) Zhao, X.; Zhang, B.; Ai, K.; Zhang, G.; Cao, L.; Liu, X.; Sun, H.; Wang, H.; Lu, L. Monitoring Catalytic Degradation of Dye Molecules on Silver-Coated ZnO Nanowire Arrays by Surface-Enhanced Raman Spectroscopy. *J. Mater. Chem.* **2009**, *19*, 5547−5553.
(46) Lan, J.; Zhou, X.; Liu, G.; Yu, J.; Zhang, J.; Zhi, L.; Nie, G. Enhancing Photocatalytic Activity of One-Dimensional $KNbO_3$ Nanowires by Au Nanoparticles under Ultraviolet and Visible-Light. *Nanoscale* **2011**, *3*, 5161−5167.
(47) Wang, P.; Huang, B.; Qin, X.; Zhang, X.; Dai, Y.; Wei, J.; Whangbo, M.-H. Ag@AgCl: A Highly Efficient and Stable Photocatalyst Active under Visible Light. *Angew. Chem., Int. Ed.* **2008**, *47*, 7931−7933.
(48) Zhu, M.; Chen, P.; Liu, M. Graphene Oxide Enwrapped Ag/AgX (X = Br, Cl) Nanocomposite as a Highly Efficient Visible-Light Plasmonic Photocatalyst. *ACS Nano* **2011**, *5*, 4529−4536.
(49) An, C.; Peng, S.; Sun, Y. Facile Synthesis of Sunlight-Driven AgCl:Ag Plasmonic Nanophotocatalyst. *Adv. Mater.* **2010**, *22*, 2570−2574.
(50) Jiang, J.; Zhang, L. Rapid Microwave-Assisted Nonaqueous Synthesis and Growth Mechanism of AgCl/Ag, and Its Daylight-Driven Plasmonic Photocatalysis. *Chem.—Eur. J.* **2011**, *17*, 3710−3717.
(51) Jiang, J.; Li, H.; Zhang, L. New Insight into Daylight Photocatalysis of AgBr@Ag: Synergistic Effect between Semiconductor Photocatalysis and Plasmonic Photocatalysis. *Chem.—Eur. J.* **2012**, *18*, 6360−6369.
(52) Han, L.; Xu, Z.; Wang, P.; Dong, S. Facile Synthesis of a Free-standing Ag@AgCl Film for a High Performance Photocatalyst and Photodetector. *Chem. Commun.* **2013**, *49*, 4953−4955.
(53) Hu, C.; Peng, T.; Hu, X.; Nie, Y.; Zhou, X.; Qu, J.; He, H. Plasmon-Induced Photodegradation of Toxic Pollutants with Ag−AgI/Al_2O_3 under Visible-Light Irradiation. *J. Am. Chem. Soc.* **2010**, *132*, 857−862.
(54) Yu, H.; Liu, L.; Wang, X.; Wang, P.; Yu, J.; Wang, Y. The Dependence of Photocatalytic Activity and Photoinduced Self-Stability of Photosensitive AgI Nanoparticles. *Dalton Trans.* **2012**, *41*, 10405−10411.
(55) Zhu, M.; Chen, C.; Chen, P.; Lei, B.; Ma, W.; Liu, M. Sunlight-Driven Ag−$AgCl_{1-x}Br_x$ Photocatalysts: Enhanced Catalytic Performances via Continuous Bandgap-Tuning and Morphology Selection. *Phys. Chem. Chem. Phys.* **2013**, *15*, 12709−12716.
(56) Zhu, M.; Chen, P.; Liu, M. Sunlight-Driven Plasmonic Photocatalysts Based on Ag/AgCl Nanostructures Synthesized via an Oil-in-water Medium: Enhanced Catalytic Performance by Morphology Selection. *J. Mater. Chem.* **2011**, *21*, 16413−16419.
(57) Wang, H.; Yang, J.; Li, X.; Zhang, H.; Li, J.; Guo, L. Facet-Dependent Photocatalytic Properties of AgBr Nanocrystals. *Small* **2012**, *8*, 2802−2806.
(58) Wang, P.; Huang, B.; Lou, Z.; Zhang, X.; Qin, X.; Dai, Y.; Zheng, Z.; Wang, X. Synthesis of Highly Efficient Ag@AgCl Plasmonic Photocatalysts with Various Structures. *Chem.—Eur. J.* **2010**, *16*, 538−544.
(59) Zhu, M.; Chen, P.; Liu, M. Highly Efficient Visible-Light-Driven Plasmonic Photocatalysts Based on Graphene Oxide-Hybridized One-Dimensional Ag/AgCl Heteroarchitectures. *J. Mater. Chem.* **2012**, *22*, 21487−21494.
(60) Wang, H.; Gao, J.; Guo, T.; Wang, R.; Guo, L.; Liu, Y.; Li, J. Facile Synthesis of AgBr Nanoplates with Exposed {111} Facets and Enhanced Photocatalytic Properties. *Chem. Commun.* **2012**, *48*, 275−277.
(61) Wang, P.; Huang, B.; Dai, Y.; Whangb, M.-H. Plasmonic Photocatalysts: Harvesting Visible Light with Noble Metal Nanoparticles. *Phys. Chem. Chem. Phys.* **2012**, *14*, 9813−9825.
(62) Zhu, M.; Chen, P.; Ma, W.; Lei, B.; Liu, M. Template-Free Synthesis of Cube-like Ag/AgCl Nanostructures via a Direct-Precipitation Protocol: Highly Efficient Sunlight-Driven Plasmonic Photocatalysts. *ACS Appl. Mater. Interfaces* **2012**, *4*, 6386−6392.
(63) Wang, H.; Lang, X.; Gao, J.; Liu, W.; Wu, D.; Wu, Y.; Guo, L.; Li, J. Polyhedral AgBr Microcrystals with an Increased Percentage of Exposed {111} Facets as a Highly Efficient Visible-Light Photocatalyst. *Chem.—Eur. J.* **2012**, *18*, 4620−4626.
(64) Zhu, M.; Chen, P.; Liu, M. High-Performance Visible-Light-Driven Plasmonic Photocatalysts Ag/AgCl with Controlled Size and Shape Using Graphene Oxide as Capping Agent and Catalyst Promoter. *Langmuir* **2013**, *29*, 9259−9268.

(65) Zhu, M.; Chen, P.; Liu, M. Ag/AgBr/Graphene Oxide Nanocomposite Synthesized via Oil/Water and Water/Oil Microemulsions: A Comparison of Sunlight Energized Plasmonic Photocatalytic Activity. *Langmuir* **2012**, *28*, 3385−3390.
(66) Xu, H.; Yan, J.; Xu, Y.; Song, Y.; Li, H.; Xia, J.; Huang, C.; Wan, H. Novel Visible-Light-Driven AgX/Graphite-Like C_3N_4 (X = Br, I) Hybrid Materials with Synergistic Photocatalytic Activity. *Appl. Catal., B* **2013**, *129*, 182−193.
(67) Feng, S.; Xu, H.; Liu, L.; Song, Y.; Li, H.; Xu, Y.; Xia, J.; Yin, S.; Yan, J. Controllable Synthesis of Hexagon-Shaped β-AgI Nanoplates in Reactable Ionic Liquid and Their Photocatalytic Activity. *Colloids Surf., A* **2012**, *410*, 23−30.
(68) Cao, J.; Xu, B.; Luo, B.; Lin, H.; Chen, S. Preparation, Characterization and Visible-Light Photocatalytic Activity of AgI/AgCl/TiO_2. *Appl. Surf. Sci.* **2011**, *257*, 7083−7089.
(69) Ghosh, S.; Saraswathi, A.; Indi, S. S.; Hoti, S. L.; Vasan, H. N. Ag@AgI, Core@Shell Structure in Agarose Matrix as Hybrid: Synthesis, Characterization, and Antimicrobial Activity. *Langmuir* **2012**, *28*, 8550−8561.
(70) Abbasi, A. R.; Morsali, A. Syntheses and Characterization of AgI Nano-structures by Ultrasonic Method: Different Morphologies under Different Conditions. *Ultrason. Sonochem.* **2010**, *17*, 572−578.
(71) Liu, Y.; Fang, L.; Lu, H.; Li, Y.; Hu, C.; Yu, H. One-Pot Pyridine-Assisted Synthesis of Visible-Light-Driven Photocatalyst Ag/Ag_3PO_4. *Appl. Catal., B* **2012**, *115−116*, 245−252.
(72) Tian, N.; Zhou, Z.-Y.; Sun, S.-G.; Ding, Y.; Wang, Z. L. Synthesis of Tetrahexahedral Platinum Nanocrystals with High-Index Facets and High Electro-Oxidation Activity. *Science* **2007**, *316*, 732−735.
(73) Greenslade, D. J.; Symons, M. C. R. Ultra-violet Spectral Studies of Silver Iodide Complex Ions. *Trans. Faraday Soc.* **1966**, *62*, 307−311.
(74) Bradley, J. N.; Greene, P. D. Potassium Iodide + Silver Iodide Phase Diagram High Ionic Conductivity of KAg_4I_5. *Trans. Faraday Soc.* **1966**, *62*, 2069−2075.
(75) Bian, S.-W.; Mudunkotuwa, I. A.; Rupasinghe, T.; Grassian, V. H. Aggregation and Dissolution of 4 nm ZnO Nanoparticles in Aqueous Environments: Influence of pH, Ionic Strength, Size, and Adsorption of Humic Acid. *Langmuir* **2011**, *27*, 6059−6068.
(76) Antonijević, M. M.; Janković, Z. D.; Dimitrijević, M. D. Kinetics of Chalcopyrite Dissolution by Hydrogen Peroxide in Sulphuric Acid. *Hydrometallurgy* **2004**, *71*, 329−334.
(77) Sokić, M. D.; Marković, B.; Živković, D. Kinetics of Chalcopyrite Leaching by Sodium Nitrate in Sulphuric Acid. *Hydrometallurgy* **2009**, *95*, 273−279.
(78) Li, Y.; Kawashima, N.; Li, J.; Chandra, A. P.; Gerson, A. R. A Review of the Structure, and Fundamental Mechanisms and Kinetics of the Leaching of Chalcopyrite. *Adv. Colloid Interface Sci.* **2013**, *197−198*, 1−32.
(79) Aydogan, S. Dissolution Kinetics of Sphalerite with Hydrogen Peroxide in Sulphuric Acid Medium. *Chem. Eng. J.* **2006**, *123*, 65−70.